Loop Closure and Intersubunit Communication in Tryptophan Synthase[†,‡]

Thomas R. Schneider,[§,||] Eva Gerhardt,[§] Minsu Lee,[⊥] Po-Huang Liang,[⊥] Karen S. Anderson,[⊥] and Ilme Schlichting*[,§]

Department for Physical Biochemistry, Max-Planck-Institute for Molecular Physiology, Rheinlanddamm 201, 44139 Dortmund, Germany, and Department of Pharmacology, Yale University School of Medicine, 333 Cedar Street, New Haven, Connecticut 06510

Received November 26, 1997; Revised Manuscript Received January 28, 1998

ABSTRACT: Crystal structures of wild-type tryptophan synthase $\alpha_2\beta_2$ complexes from *Salmonella typhimurium* were determined to investigate the mechanism of allosteric activation of the α-reaction by the aminoacrylate intermediate formed at the β-active site. Using a flow cell, the aminoacrylate (A-A) intermediate of the β-reaction ($TRPS_{A-A}^{F-IPP}$) was generated in the crystal under steady state conditions in the presence of serine and the α-site inhibitor 5-fluoroindole propanol phosphate (F-IPP). A model for the conformation of the Schiff base between the aminoacrylate and the β-subunit cofactor pyridoxal phosphate (PLP) is presented. The $TRPS_{A-A}^{F-IPP}$ structure is compared with structures of the enzyme determined in the absence (TRPS) and presence ($TRPS^{F-IPP}$) of F-IPP. A detailed model for binding of F-IPP to the α-subunit is presented. In contrast to findings by Hyde et al. [(1988) *J. Biol. Chem. 263*,-17857−17871] and Rhee et al. [(1997) *Biochemistry 36*, 7664−7680], we find that the presence of an α-site alone ligand is sufficient for loop αL6 closure atop the α-active site. Part of this loop, αThr183, is important not only for positioning the catalytic αAsp60 but also for coordinating the concomitant ordering of loop αL2 upon F-IPP binding. On the basis of the three structures, a pathway for communication between the α- and β-active sites has been established. The central element of this pathway is a newly defined rigid, but movable, domain that on one side interacts with the α-subunit via loop αL2 and on the other side with the β-active site. These findings provide a structural basis for understanding the allosteric properties of tryptophan synthase.

Tryptophan synthase (TRPS[1] EC 4.2.1.20) is an $\alpha_2\beta_2$ tetrameric enzyme complex that catalyzes the last two reactions in the biosynthesis of tryptophan (for reviews, see refs *26*, *45*, *46*, and *54*). The physiologically important reaction is termed the αβ-reaction and involves the conversion of indole 3-glycerol phosphate (IGP) and serine to tryptophan and water (*18*, *20*, *40*). The α-subunit catalyzes the cleavage of IGP to indole and glyceraldehyde 3-phosphate (G3P) (α-reaction), while the β-subunit catalyzes the condensation of indole with serine mediated by pyridoxal phosphate (β-reaction) as illustrated in Scheme 1. Tryptophan synthase is considered a classic example of an enzyme that exhibits substrate channeling, where a metabolic intermediate is transferred from one active site to another without free diffusion. The three-dimensional structure of the enzyme from *Salmonella typhimurium* provides physical evidence for a 25 Å long hydrophobic tunnel connecting the α- and β-active sites (*25*) through which the metabolic intermediate of the αβ-reaction, indole, would be transferred from the α- to the β-subunit (see Figure 1). The tunnel not only acts to direct the diffusion of indole in order to prevent its loss by diffusion through the cell membrane but also takes part in the allosteric interactions that synchronize the reactions taking place at both ends of the tunnel. In particular, the reaction of serine with the cofactor pyridoxal phosphate (PLP) of the β-site modulates the formation of indole at the α-site as well as its passage through the tunnel so that indole does not reach the β-site before a highly reactive aminoacrylate [E(A-A), see Figure 2] has been formed there. This effectively prevents the accumulation of indole at the α-site or in the tunnel. This kinetic feature, together with the very rapid diffusion of indole through the tunnel and the fast and largely irreversible reaction of indole with the aminoacrylate which forms tryptophan at the β-site, makes the bifunctional tryptophan synthase a very efficient enzyme (*6*).

The necessity to coordinate two chemical reactions over a distance of 25 Å and to control the channeling of the

[†] This work was supported by NIH Grant GM45343 (K.S.A.) and BMBF Grant 05641EH5 (I.S.).

[‡] The coordinates of the structures have been deposited with the Brookhaven Protein Data Bank (PDB entries 2wsy, 1a50, and 1a5s).

* Author to whom correspondence should be addressed.

[§] Max-Planck-Institute for Molecular Physiology.

[||] Present address: Institute of Inorganic Chemistry, University of Göttingen, Tammannstrasse 4, 37077 Göttingen, Germany.

[⊥] Department of Pharmacology, Yale University School of Medicine.

[1] Abbreviations: PLP, pyridoxal 5′-phosphate; IGP, indole 3-glycerol phosphate; G3P, glyceraldehyde 3-phosphate; IPP, indole propanol phosphate; F-IPP, 5-fluoroindole propanol phosphate; TRPS, native wild-type tryptophan synthase; $TRPS^{F-IPP}$, complex of TRPS with F-IPP; $TRPS_{A-A}^{F-IPP}$, complex of TRPS with F-IPP and L-Ser; TIM, triosephosphate isomerase; βK87T−Ser−IPP, complex of the βK87T mutant with L-Ser and IPP (61); βK87T−Ser−GP, complex of the βK87T mutant with L-Ser and G3P (61); βK87T−Ser, complex of the βK87T mutant with L-Ser (61); rms, root-mean-square; ⟨esd⟩, mean coordinate error; E(Ain), internal aldimine; $E(Aex_1)$, L-Ser external aldimine; $E(Q_1)$, quinonoidal intermediate formed from L-Ser; E(A-A), α-aminoacrylate Schiff base; E(MK), methyl ketoamine tautomer of E(A-A); NMR, nuclear magnetic resonance.

S0006-2960(97)02895-X CCC: $15.00
Published on Web 04/02/1998

Scheme 1

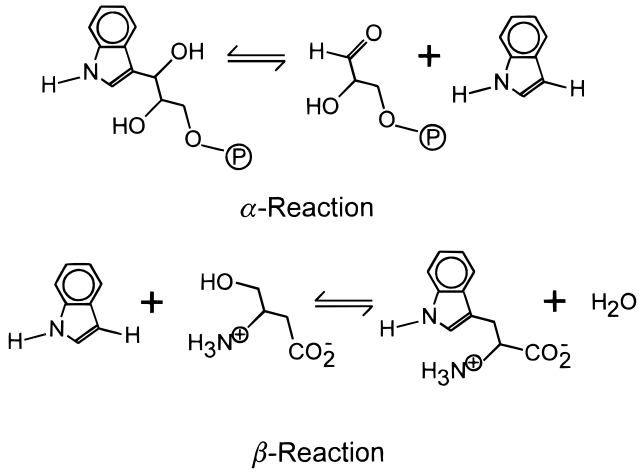

intermediate through the tunnel render tryptophan synthase an ideal system for the study of long-range allosteric interactions. Spectroscopic and kinetic studies have shown that the $\alpha_2\beta_2$ complex undergoes extensive conformational changes upon ligand binding to the α-site (*4*, *15*, *53*, *66*). One component of these conformational changes has been identified as the ordering and closure of a flexible surface loop atop the α-site similar to the loop closure observed in trypanosomal triosephosphate isomerase (TIM) (*15*, *38*, *61*). Besides this localized change, which seals the α-site and the corresponding end of the tunnel from solvent, ligand binding at the α-site also modulates the *β*-site so that the aminoacrylate [E-(A-A)] becomes the most favored intermediate (see Figure 2) (*3*, *42*, *47*, *56*). The formation of this highly reactive species is communicated back to the α-site and leads to a dramatic enhancement in the rate of IGP cleavage, as observed in rapid chemical quench (*6*) and rapid scanning stopped-flow experiments (*13*, *37*). Additional evidence for the importance of the aminoacrylate complex for intersubunit communication is provided by a mutant of tryptophan synthase in which the lysine involved in the Schiff base formation with PLP is replaced by a threonine residue (*β*K87T). In this mutant, the aminoacrylate can be created only by a "chemical rescue" method (*39*); otherwise, the *β*-reaction does not proceed further than the formation of the external aldimine [E(Aex_1), Figure 2]. The marginal activation of the α-reaction in the mutant enzyme (*7*) indicates an unfavorable effect of the mutation on intersubunit communication. The most intriguing questions arising from the wealth of available data include the nature of the reciprocal communication from the α- to the *β*-site and the structural changes that control the passage of indole through the tunnel. It is believed that the tunnel is opened by movement of two aromatic residues (*β*Tyr279 and *β*Phe280) that are anchored in the tunnel wall and are thought to act as a molecular gate (*14*, *60*, *63*, *67*). Key steps in answering these questions are crystal structures of complexes representing intermediate states occurring during the reaction.

At present, the structures of the unliganded native enzyme at 2.5 Å resolution and the native structure in the presence of monovalent cations (*25*, *61*) are available. The crystal structures of four enzyme−ligand complexes of the *β*K87T mutant containing external aldimines at the *β*-site have been determined recently (*61*) and have provided valuable insight into the structural basis of intersubunit communication. However, the structural changes related to the formation of aminoacrylate at the *β*-site still remain to be elucidated.

Crystals of tryptophan synthase are catalytically active (*2*). Mozzarelli et al. have demonstrated that wild-type TRPS can bind substrates in the crystalline state and that ligands bound to the α-site alter the distribution of intermediates formed at the *β*-site (*47*). Nonhydrolyzable analogues of α-site substrates, such as indole propanol phosphate (IPP; *32*), can be introduced into crystals of tryptophan synthase by soaking (*25*, *47*) or cocrystallization, and intermediates of the *β*-reaction can be produced and crystallographically observed under steady state conditions in a flow cell. In particular, in the presence of an α-site inhibitor, the aminoacrylate can be accumulated at the *β*-site (*47*, *56*, *73*).

In this work, we have determined the crystal structure ($TRPS_{A-A}^{F-IPP}$) of the aminoacrylate intermediate of wild-type TRPS under steady state conditions in the presence of the α-ligand 5-fluoroindole propanol phosphate (F-IPP). In addition, we have determined the structures of wild-type TRPS in the absence of the *β*-site ligand, both with and without F-IPP ($TRPS^{F-IPP}$ and TRPS, respectively). We present a detailed description of these structures and a comparison with related structures of the mutant *β*K87T. We derive a detailed structural model for the $\alpha \leftrightarrow \beta$ communication. A critical test for the model is the ability to explain how the presence of a ligand at the α-active site shifts the equilibrium at the *β*-active site to the aminoacrylate intermediate. Thus, the structural study serves as a basis for a better understanding of functional and structural aspects of allosteric interactions and substrate channeling between the active sites of the bifunctional tryptophan synthase $\alpha_2\beta_2$ complex.

MATERIALS AND METHODS

Synthesis of 5-Fluoroindole Propanol Phosphate. 5-Fluoroindole propanol phosphate (F-IPP) was synthesized by condensing 5-fluoroindole with acrylic acid to form the indolylnitrile that was subsequently hydrolyzed to produce the 5-fluoroindolyl propionic acid (*27*). This was reduced with lithium aluminum hydride to form 5-fluoroindolyl propanol. The alcohol was converted to the phosphate by treatment with 2-cyanoethyl phosphate, pyridine, and dicyclocarbodiimide (*28*, *32*, *68*). Treatment with ammonium hydroxide and anion exchange chromatography gave the ammonium salt of the desired F-IPP. The structure of the final compound was verified by ^{1}H-NMR,^{13}C-NMR, ^{19}F-NMR, ^{31}P-NMR, mass spectroscopy, and HPLC.

Fluorescence Titration Experiments. The K_d value for interaction of F-IPP with tryptophan synthase was determined as previously described (*19*, *21*). Measurements were performed using an SLM 4800 fluorimeter (Urbana, IL) at 25 °C. The excitation wavelength was 305 nm (1 nm band-pass), and the emission (8 nm band-pass) was 320 nm. The decrease in intrinsic fluorescence of a solution of TRPS was monitored by titrating in a solution of F-IPP. The fluorescence intensity was recorded as the average of four 10 s readings, and three independent experiments were carried out. The data were fit to a quadratic equation relating the observed fluorescence to the concentration of bound ligand as previously described (*5*) using nonlinear regression on a Macintosh computer with the KaliedaGraph curve-fitting program (Synergy Software).

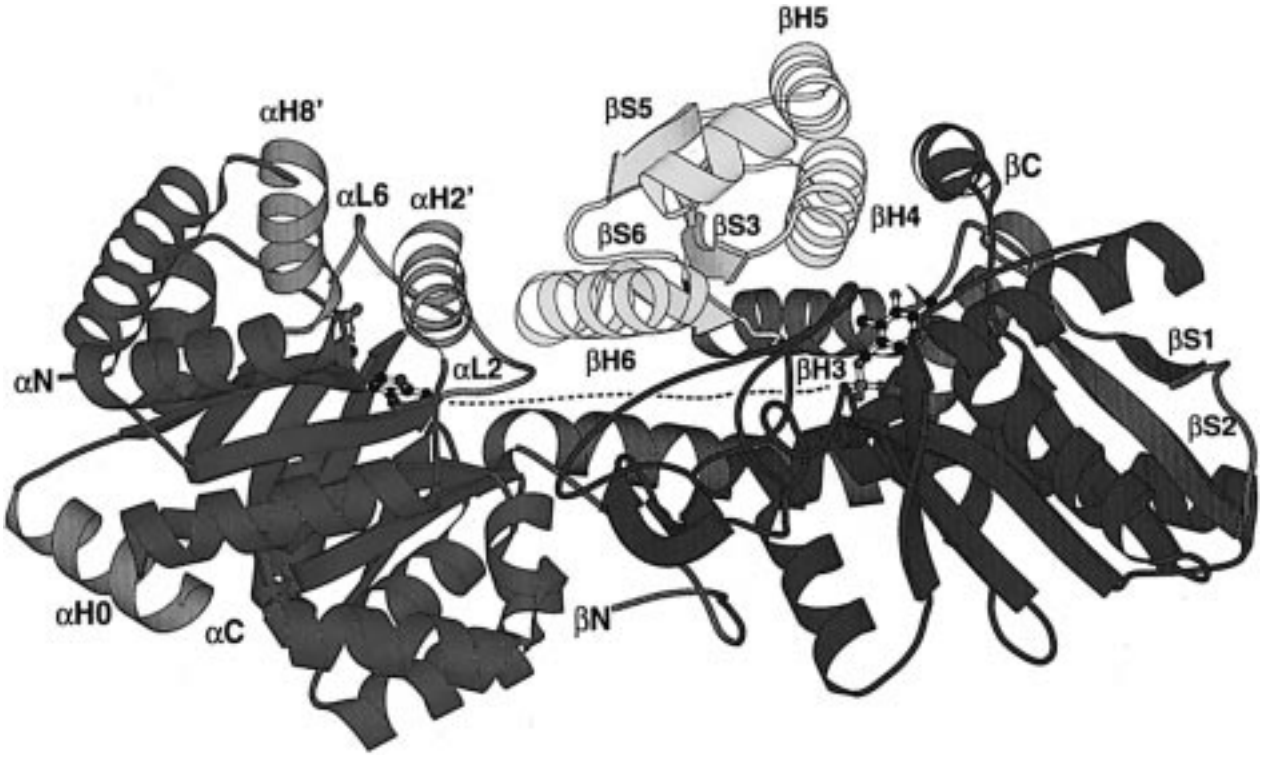

FIGURE 1: Schematic representation of the overall fold of the $\alpha\beta$-dimer based on $TRPS^{F-IPP}$. F-IPP and PLP bound to the α- and β-subunit are represented by balls and sticks. The tunnel connecting the α- and β-sites is indicated by a dashed line. The figure was prepared using MOLSCRIPT (*34*). The α- and β-reactions are shown in Scheme 1.

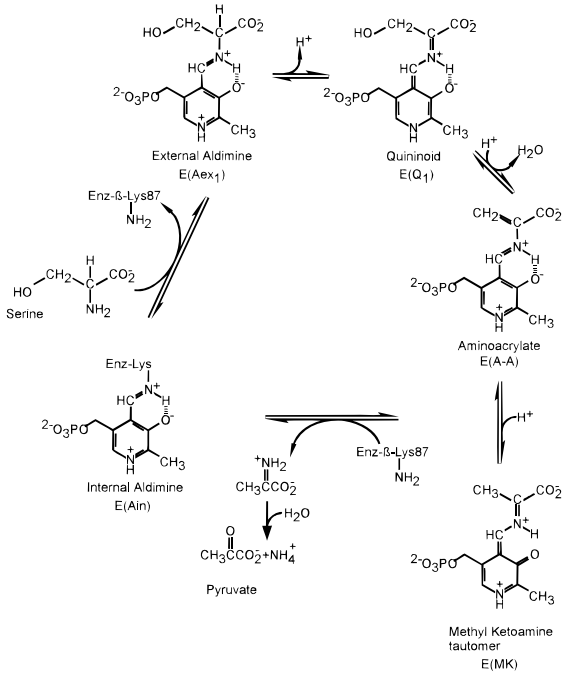

FIGURE 2: Reactions at the active site of the β-subunit. In the absence of L-Ser, PLP is covalently bond to βLys87 [E(Ain)]. When L-Ser binds, the amino group of serine replaces the ϵ-amino group of the lysine forming an external aldimine [$E(Aex_1)$]. This is followed by a deprotonation step which leads to a quinoid [$E(Q_1)$], which subsequently is protonated and then loses water which leads to an aminoacrylate [E(A-A)], which is in equilibrium with a methyl ketoamine tautomer [E(MK)]. In the absence of indole, the aminoacrylate slowly hydrolyzes to pyruvate and ammonia.

Crystallization and Introduction of Substrates. The tryptophan synthase $\alpha_2\beta_2$ complex from *S. typhimurium* was crystallized by mixing 5 μL of the enzyme solution [10 mg/mL TRPS in 50 mM bicine (pH 7.8), 1 mM EDTA, 5 mM dithioerythritol, and 20 μM pyridoxal phosphate] with 5 μL of the reservoir solution [50 mM bicine (pH 7.8), 1−2 mM spermine, and 10% PEG 8000] and equilibrating the drops against the latter using hanging drop geometry (*1*). The crystallization setups were kept in the dark at room temperature. Monoclinic crystals grew within 2 weeks and belong to the space group *C*2 with one $\alpha\beta$-dimer in the assymetric unit and unit cell dimensions as given in Table 1. The F-IPP complex of TRPS was obtained by cocrystallization in the presence of 0.4 mM F-IPP. The crystals of $TRPS^{F-IPP}$ are isomorphous to those of the native enzyme. The aminoacrylate complex of TRPS ($TRPS^{F-IPP}_{A-A}$) was generated by mounting a $TRPS^{F-IPP}$ crystal in a flow cell (0.7 mm in diameter) using pipe cleaner fibers to immobilize the crystal (*57*, *72*). We chose to work at pH 7.0 since the decay of the aminoacrylate to pyruvate and ammonia is pH-dependent. A solution containing 100 mM Na-Hepes (pH 7.0), 20 μM PLP, 0.4 mM F-IPP, 5 mM dithioerythritol, 20% PEG 8000, and 200 mM L-Ser (pH adjusted to 7.0 with NaOH) was passed across the crystal at a flow rate of ca. 5 μL/min. Data collection was started 30 min after initiating the flow.

X-ray Data Collection. Diffraction data were collected at 4 °C on beamline BW7B at EMBL c/o DESY (*65*) (TRPS) and on beamline X12C at the NSLS ($TRPS^{F-IPP}$ and $TRPS^{F-IPP}_{A-A}$) at wavelengths of 0.86 and 1.15 Å, respectively, using a MAR detector. The crystal to detector distance was 250 mm (TRPS) or 264 mm ($TRPS^{F-IPP}$ and $TRPS^{F-IPP}_{A-A}$). Data were processed using the *hkl* suite of programs (*52*). The data statistics are given in Table 1.

Refinement. The starting model used for all three refinements was the coordinate set of native TRPS [PDB entry

Table 1: Crystal Parameters, Data Collection, and Refinement Statistics

	TRPS	$TRPS^{F-IPP}$	$TRPS^{F-IPP}_{A-A}$
crystal parameters			
unit cell ($a \times b \times c$) (Å)	185.1 × 61.2 × 67.6	182.8 × 60.7 × 67.5	182.7 × 60.8 × 67.5
unit cell (β) (deg)	94.7	94.5	94.6
data statistics			
resolution (Å)	10.0−3.05	26.90−2.30	30.0−2.30
no. of collected refections	28 423	66 781	68 449
no. of unique reflections	13 162	31 823	31 198
compl. (total/high) (%)[a]	90.9/94.7	95.6/91.6	93.8/89.8
R_m (total/high) (%)[b]	3.4/5.6	6.0/13.1	6.7/20.7
$\langle I/\sigma(I)\rangle$ (total/high)	20.2/11.8	13.4/6.4	13.5/4.2
refinement statistics			
resolution range (Å)	10.0−3.05	10.0−2.29	10−2.30
no. of reflections with $F > 2\sigma(F)$	12 850	31 627	30 327
no. of protein atoms[c]	4632	4919	4992
no. of waters	0	238	116
no. of others[d]	16	34	40
bulk solvent (k/B) ($eÅ^{-3}/Å^2$)	0.37/46.2	0.37/41.2	0.39/66.6
R_{work}, R_{free} (%)[e]	19.7/29.9	16.2/22.1	17.7/24.7
R_{cryst} (%)[f]	20.2	16.4	18.1
rmsd for bonds/angles (Å/deg)	0.003/0.9	0.006/1.3	0.006/1.3
disallowed (Φ, Ψ)[g]	βArg275	αPhe212	αPhe212
$\langle B\rangle$ (mc/sc/wat) ($Å^2$)[h]	20.4/20.9/−	17.5/20.9/25.4	23.8/26.8/23.8
⟨esd⟩ (Å)	0.37	0.21	0.27

[a] Completeness, R_m, and $\langle I/\sigma(I)\rangle$ are given for all data and for data in the highest-resolution shell. [b] $R_m = \sum|I - \langle I\rangle|/\sum I$. [c] No unambigous electron density was found for the following residues in the respective models: TRPS, α54−62, α177−195, αPhe212, α249−250, β139−142, β158−165, β389−397; $TRPS^{F-IPP}$, α1, α188−193, α268, β1, β394−397; and $TRPS^{F-IPP}_{A-A}$, α1, α188−195, α268; β1−2, β390−397. [d] Other atoms correspond to one Na^+ cation in all cases and PLP in TRPS, F-IPP, and PLP in $TRPS^{F-IPP}$, and F-IPP, PLP, and aminoacrylate in $TRPS^{F-IPP}_{A-A}$. [e] For definition of R_{work} and R_{free}, see Materials and Methods. [f] $R_{cryst} = \sum||F_o| - |F_c||/\sum|F_o|$. [g] Combinations of Φ and Ψ angles that fall into the disallowed region of the Ramachandran plot as defined in PROCHECK. [h] Mean values are given for main chain (mc) and side chain (sc) atoms and water molecules (wat).

1WSY (*9*, *25*)] omitting the cofactor PLP. X-PLOR(online) 3.851 (*11*) was employed for all calculations and the graphics program O (*30*) was used for map interpretation ($3F_{obs} - 2F_{calc}$ and $F_{obs} - F_{calc}$ difference syntheses at varying contour levels) and manual rebuilding. The strategy used was essentially the same for all three refinements. After an initial round of refining the α- and β-subunit as rigid bodies, the model was subjected to a simulated annealing protocol starting at 3000 K to remove model bias (*22*). The resulting model was inspected carefully and suspicious regions were omitted for later rebuilding. Several rounds of slow cooling protocols with varying weights and starting temperatures, individual *B*-factor refinement, and manual rebuilding followed. In contrast to common practice, the *B*-factors for the low-resolution data set (TRPS, $d_{min} = 3.05$ Å) were not refined in groups but individually with tight restraints ($\sigma_B = \sigma_A = 0.5$ $Å^2$) for neighboring atoms, except C_α atoms ($\sigma_B = 1.5$, $\sigma_A = 2.5$). Placement of water molecules (only in the refinements of $TRPS^{F-IPP}$ and $TRPS^{F-IPP}_{A-A}$) was done mostly automatically by selecting the peaks in $F_{obs} - F_{calc}$ difference maps that had heights greater than 4.5σ and fulfilled hydrogen bonding criteria. Water molecules were rejected when their *B*-factors became greater than an arbitrary threshold of 45 $Å^2$ upon refinement. After automatic water placement, all remaining peaks with abs(peakheight) values of $\geq 5.0\sigma$ were inspected systematically. A two-parameter bulk solvent correction (*29*) was applied throughout and recalculated after each round of rebuilding. In the final stages of the refinement conjugate gradient refinements of coordinates and *B*-factors were carried out. The refinements were considered complete when no more interpretable peaks higher than 5.0σ were found in a $F_{obs} - F_{calc}$ difference map. In each of the structures, a Na^+ ion was located in difference density maps ligated to the carbonyl oxygens of βPhe306, βSer308, Gly232, and two water molecules as described by Rhee et al. (*60*).

Structure Comparisons. Mean coordinate errors ⟨esd⟩, were estimated by using the σ_A method (*59*). To reduce bias introduced by subjective choice of atoms for least-square superposition of the various models, difference distance matrices for C_α atoms, Δ_{ij}, were calculated between models. Only matrix elements with Δ_{ij} of $> \sqrt{(\langle esd\rangle_a^2 + \langle esd\rangle_b^2)}$, where a and b stand for two different models, were considered significant and included in a graphical representation. Then superpositions were performed on the basis of the parts classified as rigid by visual inspection of the matrices.

RESULTS AND DISCUSSSION

Quality of the Models. All three models are of high quality as reflected in the low values for R_{free} and the small mean deviations of geometrical parameters from their ideal values (Table 1). The mean values for individual isotropic *B*-factors and the mean coordinate errors are within the expected range. In all three structures, there are only three cases for which the backbone dihedral angles fall into the disallowed region of the Ramachandran plot (*36*, *58*). In the first case, βArg275 in TRPS, the electron density does not allow an unambigous placement for both neighboring peptide planes. The other two cases concern residue αPhe212, which is flanked by glycine residues on either side and whose side chain is invisible in TRPS. In $TRPS^{F-IPP}$ and $TRPS^{F-IPP}_{A-A}$, the aromatic ring of αPhe212 is involved in binding of the substrate analogue, leading to a strained conformation of the main chain dihedrals.

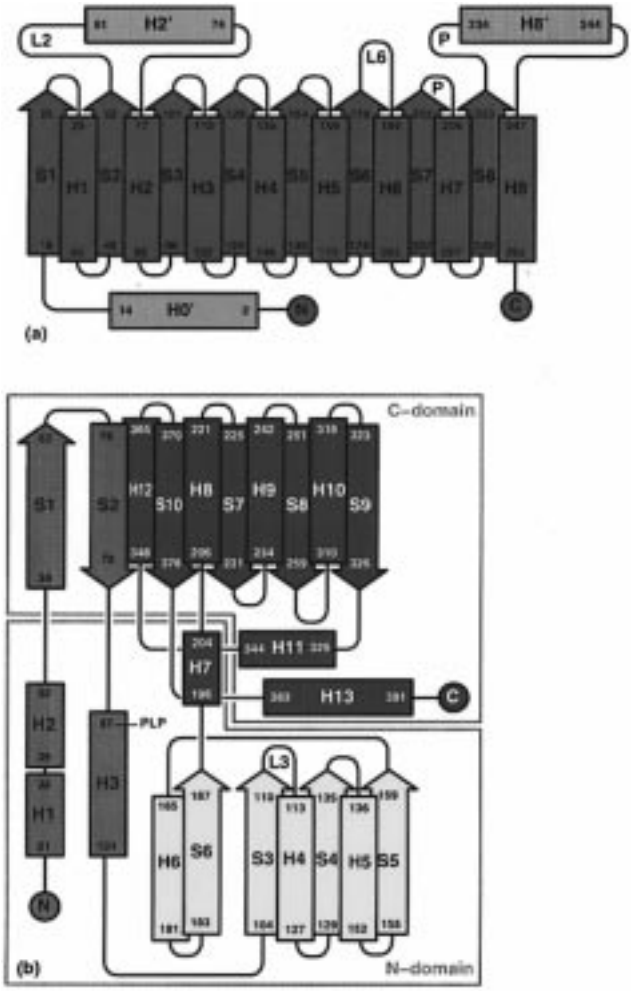

FIGURE 3: Schematic view of the topology of the α- and β-subunit (panels a and b, respectively) of the tryptophan synthase $\alpha\beta$ complex. The color coding is identical to that used in Figure 1; β-sheets are shown as arrows and α-helices as rectangles. Numbers of starting and ending residues of secondary structure elements are given as determined by PROCHECK (*31*, *36*). The color coding in panel a is as follows: red for the canonical $\alpha\beta$-barrel part of the α-subunit and light red for extensions. In panel b, the domain wrapping around the redefined C domain (shown in blue) is shown in light blue, and the newly defined COMM domain (see the text) is shown in yellow. In both panels, important loop regions are marked as L2, L6, and L3, respectively. Loop regions involved in phosphate binding at the α-site are marked by P. For the β-subunit, the division into domains as given in Hyde et al. (*25*) is indicated by gray boxes. In the text, secondary structure elements of the α- and β-subunit are referred to with prefixes α and β, respectively.

Architecture of the $\alpha\beta$ Complex. The secondary and tertiary structure of the complex is the same with respect to the three different states of the enzyme investigated here. The following description of the the overall structure of the complex is based on the most accurate model, $TRPS^{F-IPP}$. Although the beginnings and ends of secondary structure elements deviate in several cases, the overall topology (Figure 3) is equivalent to the one described by Hyde et al. (*25*). However, on the basis of functional and topological considerations, we introduce a division of the β-subunit into domains, which is substantially different from the definition by Hyde et al. and similar to the one suggested by Rhee et al. (*61*) (Figures 1 and 3).

The fold of the α-subunit is that of a canonical eight-fold $\alpha\beta$-barrel with several structural elements added. At the N terminus of the α-subunit, an α-helix (αH0) is attached to the bottom, i.e. the side opposite the active site, of the barrel. On the top of the barrel, the $\alpha\beta$-barrel structure is supplemented in three locations. Between strand αS2 and helix αH2, an α-helix (helix αH2′) preceded by a loop (loop αL2) is inserted. The latter loop contains several residues that play key roles in catalysis and intersubunit communication (ref *46* and below). Another important loop (loop αL6) is found between strand αS6 and helix αH6 in a position which is topologically equivalent to the position of the flexible loop in TIM (*69*). Finally, an additional helix (αH8′), oriented with its N terminus toward the phosphate binding site, is inserted before helix αH8.

At present, the β-subunit of TRPS represents a unique fold. No close similarities were detected by a DALI search (*23*), and no equivalent folds are listed in the current release of SCOP (*48*). Hyde et al. have described the fold of this subunit in terms of two nearly equally sized and topologically similar domains (*25*). These were named the N- and the C domain [residues $\beta1-\beta204$ and residues $\beta205-\beta397$, respectively, with a short piece of the N domain (residues $\beta53-\beta85$) crossing over into the C domain (Figure 3)]. On the basis of the results of this study, we suggest a different division of the β-subunit into domains. Both N-terminal helices (βH1 and βH2), the crossover domain, and the following helix βH3 wrap around the C domain (redefined to comprise residues $\beta190-\beta397$). This N-terminal domain is anchored to the protein by coupling of β-strands βS1 and βS2 (the previous crossover domain) to the central β-sheet of the C domain on one end and interactions between residues $\beta7-\beta16$ and $\beta275-\beta286$ of the C domain on the other end. The remaining part of the previous N domain (residues βGly102$-\beta$Gly189) constitutes a domain that has only very few interactions with the rest of the protein. As will be shown below, this domain plays an important role in the allosteric communication between the α- and the β-site, and therefore, we name it the COMM domain. Apart from being nine residues shorter at its N-terminal end, this definition of the COMM domain is identical to that of the mobile region (residues βGly93$-\beta$Gly189) introduced by Rhee et al. (*61*).

Native Structure. The model for TRPS contains 612 out of 665 residues, i.e. 21 residues less than the preliminary model of TRPS deposited in the protein data bank [1WSY (*9*, *25*)]. This is due to the lower resolution of our data and the use of very stringent criteria for chain tracibility. The parts of the protein that were not modeled, clearly, have more than one conformation when the respective electron densities are compared to those corresponding to ordered parts. In the α-subunit, the following regions are missing from our model: αL2, α54−α62 (α56−α58 in 1WSY) and αL6, α177−α195 (α178−α191 in 1WSY); αPhe212 was omitted from the model as there was no electron density for this residue, which is flanked by glycines on both sides. αLys249 and αGly250 in αH8 are missing from our model, but were modeled in 1WSY. The following residues of the β-subunit are not included in our model: βVal139$-\beta$Gln142 in the loop region between βS4 and βH5 (the secondary element assigment is based on 1WSY), βPro158$-\beta$Thr165 in the loop region between βS5 and βH6, and the C terminus of the β-subunit from β389 onward. After superposition using 506 C_α atoms with B values < 35 Å^2 in TRPS, the rms difference

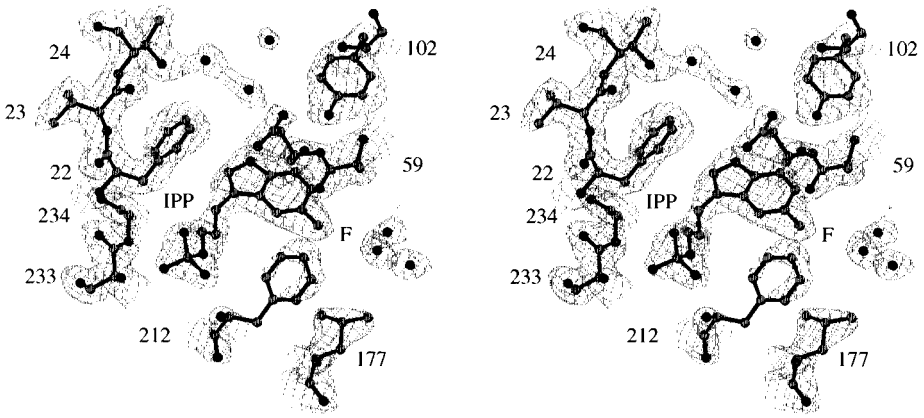

FIGURE 4: Simulated annealing $2F_{obs} - F_{calc}$ σ_A-weighted omit map (*22*, *59*), contoured at the σ level, around the F-IPP bound to the α-site. Two hundred twenty-one atoms, including F-IPP and those in the vicinity of it, were omitted before the map calculation. The figure was prepared using BOBSCRIPT (*75*).

between positions of equivalent C_α atoms is 0.64 Å, indicating that, within the limits of the combined coordinate errors, the two models are identical in the well-defined regions of the polypeptide chain.

Binding of F-IPP to the α-Site. Apart from residues at the termini of both polypeptide chains, the only part of the $TRPS^{F-IPP}$ complex that remains too disordered to be built into electron density is the C-terminal part of loop αL6 (αArg188−αLeu193).

In addition to the localization of the binding site, the highly refined structure of TRPS with F-IPP bound ($TRPS^{F-IPP}$) gives a very detailed view of the interactions between the inhibitor and the protein residues in the vicinity of it (Figure 4). As previously described for the binding of IPP to the wild-type enzyme (*25*) and to the mutant *β*K87T (*61*), F-IPP binds in a depression on the surface of the α-subunit that offers several hydrogen bonds to the phosphate group at one end and a hydrophobic environment to accommodate the indole moiety at the other end (Figure 5). The binding of the phosphate group of F-IPP takes place in a region of the α-subunit that is topologically equivalent to the phosphate binding sites of several other α*β*-barrel enzymes (*70*). In fact, the local geometry of binding of the F-IPP phosphate group is almost identical to that of the respective region where G3P binds to TIM (*51*). The N terminus of helix αH8′ (αGly234−αSer235−αAla236) provides direct and water-mediated hydrogen bonds to the phosphate oxygen atoms OP1 and OP2 (Figure 6). It has been suggested that the dipole of this helix provides a positive electrostatic field supplementing or fine tuning the phosphate binding capability of this site (*25*, *64*). Loop αL7 (αGly211−αPhe212−αGly213−αIle214) has been found to be absolutely conserved in a number of sequences encoding TRPS α-subunits in different species (*17*) and not only provides hydrogen bonding partners for OP2 and OP3 but also interacts with the indole moiety of the inhibitor via the aromatic ring of αPhe212, which lies on top of the indole in an edge-to-face arrangement (*16*). The two glycine residues flanking αPhe212 act as hinges, rendering this residue very flexible and facilitating both substrate entry and binding. Their importance is reflected in being either a site of missense mutation (Gly211) or a site of a second-site revertant (Gly213) (*45*). The third part of the α-subunit interacting with the phosphate oxygens of F-IPP is mobile loop αL6, most of which

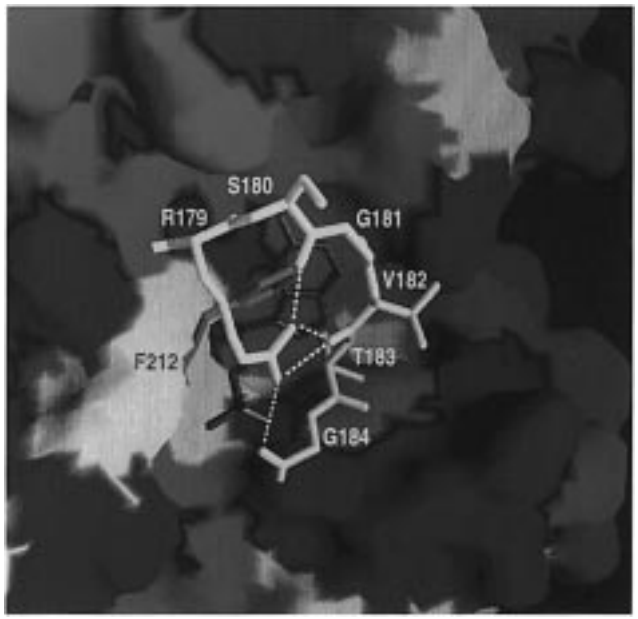

FIGURE 5: α-Subunit substrate binding. The surface of the α-subunit is shown in red (hydrophobic), blue (polar), and white (others). F-IPP is represented by gray sticks at the bottom of the binding pocket. αPhe212 (green) is sandwiched between the indole moiety of F-IPP and loop αL6 in its closed conformation (residues αArg179−αGlu184 are shown as yellow sticks, hydrogen bonds as thin yellow lines). The figure was prepared using the program GRASP (*50*).

becomes ordered upon substrate binding in a way similar to the loop closure observed in TIM (*69*). In the closed state, loop αL6 forms an almost circular lid, stabilized by a number of hydrogen bonds originating from the guanidinium group of αArg179 and extending radially like spokes, sandwiching αPhe212 onto the indole moiety of F-IPP (Figures 5 and 6). Replacement of αArg179 by other amino acids will clearly disrupt the structure of this wheel-like arrangement, explaining the lower substrate-binding affinity observed by Brzovic et al. for the mutant αR179L (*15*). On the protein side, the fluoroindole moiety of the inhibitor fits well into the hydrophobic pit lined by residues αPhe22, αIle64, αLeu100, αTyr102, αLeu127, αIle153, and αTyr175, residues previously found to interact with the hydrophobic part of IPP by Hyde et al. and Rhee et al. (*26*, *61*). We chose to study F-IPP as opposed to IPP since it offers the possibility of ^{19}F-NMR investigations [see studies using 5-fluoro-L-tryp-

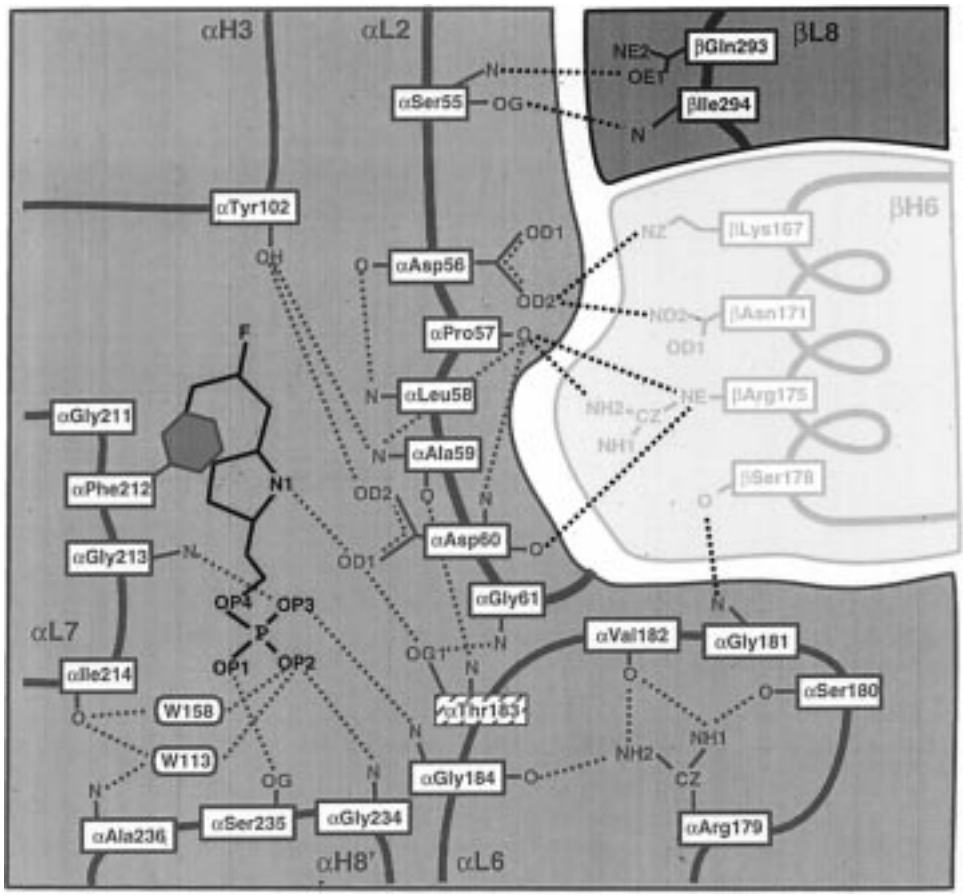

FIGURE 6: Schematic view of hydrogen bonds (broken lines) present after binding of F-IPP to TRPS. Hydrogen bonds within the α-subunit (red background) are shown in red. Interactions across the interface between the α- and the β-subunit (blue and yellow background, where yellow indicates parts of the COMM domain) are shown in black.

tophan (*44*)]. In the $TRPS^{F-IPP}$ and $TRPS^{F-IPP}_{A-A}$ structures, the fluorine atom points toward $C_{\delta 1}$ of αIle153. Since no coordinates of the wild-type tryptophan synthase IPP complex are available, we cannot determine the influence of the fluorine atom on the protein structure.

In contrast to the conclusion drawn by Rhee et al. that both the α- and the β-site have to be occupied with substrate to induce closure of loop αL6, we find that binding of F-IPP alone suffices to trigger the simultaneous ordering of loops αL6 and αL2. Although binding of F-IPP to wild-type TRPS is slightly tighter than binding of IPP, as indicated by the K_d values (0.2−0.5 vs 1−2 μM, data not shown), it is unlikely that the additional fluorine atom leads to a significantly different binding of the substrate analogue to the wild-type enzyme. It cannot be excluded that the different behavior of the βK87T mutant protein in terms of loop closure at the α-site is an indirect consequence of the mutation performed at the β-site.

Concerning the α-reaction, the TRPS structure supports a general "push−pull" acid−base mechanism for the reversible cleavage of the $C_3'-C_3$ bond of indole 3-glycerol phosphate, in which αAsp60 and αGlu49 act as bases (*33*, *49*). The carboxylate group of αAsp60 forms a strong hydrogen bond to the nitrogen atom of the indole moiety (2.7 Å), thus allowing abstraction of the respective proton or a tautomerization of the indole ring. The carboxylate group of αGlu49 is located in the vicinity of the indole moiety surrounded by sufficient space to allow the transfer of a proton from glycerol phosphate to indole as suggested by Nagata et al. (*49*). Besides its importance for the α-reaction itself, the interaction between the carboxylate of αAsp60 and F-IPP-N1, together with three hydrogen bonds involving αThr183 (αThr183-$O_{\gamma 1}\cdots$αAsp60-$O_{\delta 1}$, αThr183-$O_{\gamma 1}\cdots$αGly61-N, and αThr183-N$\cdots$αAla59-O) may form the basis for the concomitant ordering of loops αL2 and αL6 upon substrate binding. A prominent role for αThr183 is supported by the fact that single amino acid substitutions at this site result in complete inactivity of the enzyme toward IGP (*74*).

Communication of Substrate Binding from the α- *to the* β*-Site.* The ordering and mutual stabilization of αL6 and αL2 upon binding of F-IPP substantially change the intersubunit interface. In addition to the interactions facilitating subunit association, new, mainly polar, interactions connecting loop αL2 of the α-subunit and helix βH6 of the β-subunit are established (Table 2 and Figure 6): αAsp56-$O_{\delta 2}\cdots\beta$Lys167-N_ζ, αAsp56-$O_{\delta 2}\cdots\beta$Asn171-$N_{\delta 2}$, αPro57-O$\cdots\beta$Arg175-N_ϵ, αPro57-O$\cdots\beta$Arg175-$N_{\eta 2}$, αAsp60-O$\cdots\beta$Arg175-N_ϵ, and Gln65-$N_{\epsilon 2}\cdots\beta$Arg175-$N_\epsilon$. Apart from these, two other weak hydrogen bonds, αGly181-N$\cdots\beta$Ser178-O (3.4 Å) and αSer55-$O_\gamma\cdots\beta$Ile294-N (3.0 Å), are formed in other regions of the subunit interface. The formation of the above intersubunit interactions leads to an ordering and repositioning of helix βH6 (Figure 3) with the largest changes occurring at its N terminus; residues β158−β164, found to be disordered in TRPS, become ordered. Similarly, residues β139−β142, located at the N terminus of βH5, become ordered as well. All these newly ordered regions belong to the COMM domain. Inspection of the

Table 2: Polar Interactions between the COMM Domain and the Rest of the $\alpha\beta$ Complex

COMM domain atom	interacting atom	distance (Å)[a]				
		TRPS	$TRPS^{F-IPP}$	$TRPS^{F\text{-}IPP}_{A\text{-}A}$	S^{F-IPP}_{A-A}	class[b]
βLys103-N	βAla98-O	3.0	2.9	3.0		nterm
βLys103-N_ζ	βGln27-$N_{\epsilon 2}$	3.2	(4.0)	3.2		nterm
βGln114-$N_{\epsilon 2}$	βGly83-O	(4.6)	3.1	(4.0)		plp
βLeu126-O	βLys99-N_ζ	3.1	(3.7)	2.7		weak
βLys167-O	βTyr279-O_η	(4.0)	3.1	3.1		gate
βLys167-N_ζ	bIle294-O	3.0	(4.5)	(4.6)		$\alpha\beta$
βLys167-N_ζ	αAsp56-$O_{\delta 2}$	−	2.8	2.8		$\alpha\beta$
βAsn171-$N_{\delta 2}$	βTyr279-O_η	3.3	2.9	3.1		gate
βAsn171-$O_{\delta 1}$	βTyr279-O_η	(3.6)	3.0	3.3		gate
βAsn171-$O_{\delta 1}$	αAsp56-$O_{\delta 2}$	−	3.0	3.0		$\alpha\beta$
βArg175-N_ϵ	αPro57-O	−	3.3	3.4		$\alpha\beta$
βArg175-N_ϵ	αAsp60-O	−	3.0	3.1		$\alpha\beta$
βArg175-N_ϵ	αGln65-$O_{\epsilon 1}$	(5.0)	3.1	3.3		$\alpha\beta$
βArg175-$N_{\eta 1}$	αPro57-O	−	2.9	3.0		$\alpha\beta$
βArg175-$N_{\eta 2}$	αGln65-$O_{\epsilon 1}$	3.2	3.4	3.3		$\alpha\beta$
βSer178-O	αGly181-N	−	3.4	3.5		$\alpha\beta$
βTyr181-O_η	αAsn157-$N_{\delta 2}$	3.1	3.3	3.3		$\alpha\beta$
βHis185-$N_{\epsilon 2}$	βGln94-$O_{\epsilon 1}$	(4.2)	2.9	3.5		cterm
βTyr186-O	βGln94-$O_{\epsilon 1}$	(3.7)	3.5	3.5		cterm
βTyr186-O	βTyr197-O_η	3.0	2.6	2.6		cterm
βLeu188-O	Gln90-$N_{\epsilon 2}$	3.2	3.0	3.0		cterm
βLeu188-O	βGln94-$N_{\epsilon 2}$	(3.9)	3.1	3.2		cterm
βLeu188-N	βGln94-$O_{\epsilon 1}$	3.2	(3.8)	(4.8)		cterm
βGly189-O	bThr190-N	2.2	2.2	2.2		cterm
βGly189-N	βThr190-N	2.9	2.9	2.9		cterm

[a] Interatomic distances of less than 3.4 Å between polar atoms are considered polar interactions, and interactions beyond this limit value are enclosed in parentheses. − indicates that an atom is not included in the respective model. [b] Interactions are classified as follows: nterm or cterm, first atom close to the N or C terminus of the COMM domain; plp, interaction with PLP positioning residue; weak, weak interaction; gate, second atom belongs to βTyr279; $\alpha\beta$, polar interaction bridging the intersubunit interface.

polar interactions originating from the COMM domain after binding of F-IPP to the α-subunit (Table 2) reveals that, apart from the hydrogen bonds bridging the subunit interface, there are only very few hydrogen bonds between the COMM domain and the rest of the enzyme that are not close to the N or C terminus of this domain. Out of these, the three hydrogen bonds between βTyr279-O_η, βLys167, and βAsn171 are particularly interesting, since they establish a link between the α-site and the pair of aromatic residues, βTyr279 and βPhe280, that are thought to have a gating function in the tunnel (see refs *14*, *60*, *63*, and *67*] and below).

Due to the lack of strong interdomain interactions, the COMM domain as a whole can be considered relatively independent from the rest of the protein. The displacement of the β109−β114 region (loop βL3) upon binding of F-IPP to the α-site (Figure 8a,b) can be explained as a consequence of the displacement of helix βH6 at the other end of the COMM domain that is communicated solely by intradomain interactions. In addition to the backbone atoms of loop βL3, the side chains of βGln114 and βGlu109 are repositioned relative to the cofactor PLP. In particular, the carboxylate group of βGlu109, which is believed to play a role in catalysis of the β-reaction (*12*), moves 1.5 Å closer to PLP. These changes at the β-site, which originate from the α-site, may be the basis for the changes in binding affinities and in the distribution of intermediates observed at the β-site upon binding of substrates to the α-site (*13*). The proposed pathway for the allosteric interaction between the α- and β-sites (α-site → αL2 → βH6 → COMM domain → β-site) is in agreement with the observation that the mutation βK167T, which breaks the salt bridge between αAsp56-$O_{\delta 2}$ and βLys167-N_ζ (Figure 6), results in a 25-fold lower rate for the β-reaction (*73*).

Binding of L-*Ser and Formation of the Aminoacrylate.* As for $TRPS^{F-IPP}$, the model for the complex between TRPS, F-IPP, and L-Ser ($TRPS^{F-IPP}_{A-A}$) contains all of the protein residues apart from residues at the termini of both polypeptide chains and the C-terminal part of loop αL6. The cofactor itself and L-Ser are clearly visible in electron density maps (Figure 7); the Schiff base linkage between βLys87 and PLP is broken, and L-Ser has been coupled to PLP. In comparison to $TRPS^{F-IPP}$, the phosphate tail of PLP is essentially in the same position, whereas the pyridoxal ring is tilted by approximately 20° about its C_5-C_2 axis (Figure 8c). Nevertheless, it cannot be derived from the electron density alone which of the intermediates occurring upon binding of L-Ser (Figure 2) is predominant under the conditions given in the crystal.

The influence of pH, temperature, and α-subunit ligands on the distribution between different intermediates at the β-site has been investigated in solution (*56*) and in the crystalline state (*47*, *62*), yielding comparable results; lower pH and/or the presence of α-site ligands strongly favors the aminoacrylate intermediate over the external aldimine. The crystalline aminoacrylate complex can be generated by passing serine across a crystal mounted in a flow cell. Under steady state conditions, the aminoacrylate will be highly populated in a $TRPS^{F-IPP}$ cocrystal since the aminoacrylate is formed at a rate of 45 s^{-1} and decays with a rate constant of only 0.2 s^{-1} to pyruvate and ammonia (*6*). To maximize the occupancy of the aminoacrylate, we chose to work at pH 7.0 since the decay of the aminoacrylate is faster at higher pH values.

In a recent study, McDowell et al. (*41*) have shown by solid state NMR spectroscopy on microcrystalline samples of TRPS that when IPP is bound to the α-site two tautomers exist simultaneously at the β-site after binding of L-Ser: the aminoacrylate Schiff base and its methyl ketoamine tautomer (Figure 2). The currently available diffraction data do not allow simultaneous refinement of both of these conformers. To account for both possibilities, we used only a single conformer and refined it without restraints on the dihedral angles of the aminoacrylate moiety while keeping all carbon atoms and the L-Ser nitrogen involved in the Schiff base linkage planar. Consequently, the resulting model does not correspond to one conformer but to a mixture of E(A-A) and E(MK).

In the current model, the aminoacrylate C_β atom points toward the tunnel and the carboxylate group is oriented toward loop βL3 (Figure 8), a region whose sequence is highly conserved in tryptophan synthases from various species (*8*, *10*, *17*). The electron density for the carboxylate group of the aminoacrylate is smeared out and in principle allows different positions of this group related by rotation about the $C_\alpha-C$ bond. This may be due in part to the simultaneous presence of the two aforementioned tautomers, but more likely corresponds to a situation with no clear energetically favorable position due to the large number of spatially close hydrogen bond donors supplied by loop βL3 and neighboring residues (Figure 8); βThr110-$O_{\gamma 1}$, βAla112-N, βGly113-N, βGln114-N, βHis115-N, and Wat51 are all

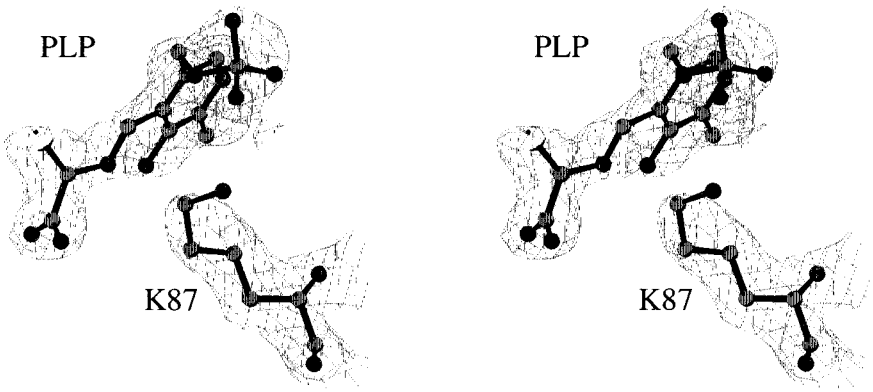

FIGURE 7: Simulated annealing $2F_{obs} - F_{calc}$ σ_A-weighted omit map (*22*, *59*), contoured at the σ level, around the β-site. Two hundred thirty-nine atoms, including, PLP, βLys87, and the aminoacrylate, were omitted before map calculation. The figure was prepared using BOBSCRIPT (*75*).

within hydrogen bonding distance from at least one of the carboxylate oxygens, independent of the rotameric state. This flexibility is in fact functionally important in allowing accomodation of different groups ligated to the C_β of the aminoacrylate without sterical problems, e.g. the external aldimines of L-Ser and L-Trp (*61*). The present conformation of the aminoacrylate not only allows favorable interactions of the aminoacrylate carboxylate group but also is consistent with the suggestion by Hur et al. (*24*) and Lu et al. (*39*) that βLys87 abstracts the α-proton from $E(Aex_1)$ to form $E(Q_1)$; for L-Ser, this conformation allows an interaction between its α-proton and βLys87, whereas for D-Ser, toward which the β-subunit shows no activity (*24*), the α-proton would be pointing away from βLys87.

After being liberated from PLP, the side chain of βLys87 moves away from the cofactor into a position where it is not solvent accessible and its N_ζ atom forms hydrogen bonds with βHis86-$N_{\epsilon 2}$ (3.1 Å) and βSer235-O_γ (3.2 Å). These findings support evidence from spectroscopic experiments that suggest the proton abstracted from is sequestered in a solvent-excluded site and possibly stored in a low-barrier hydrogen bond (*24*).

Activation of the α*-Reaction.* Kinetic investigations have shown that the formation of the aminoacrylate at the β-site activates the cleavage of IGP at the α-site and the subsequent release of indole into the tunnel (*6*, *7*, *13*). In $TRPS^{F-IPP}_{A-A}$, the overall reaction does not proceed further than the activation step, since F-IPP cannot be hydrolyzed.

Difference distance matrices for atoms indicate that the only significant difference between the polypeptide backbone of $TRPS^{F-IPP}$ and $TRPS^{F-IPP}_{A-A}$ is a rigid-body displacement of the COMM domain. This is also clearly visible when both models are superpositioned using only C_α atoms not belonging to the COMM domain. These atoms can be superimposed with an rms difference of 0.24 Å (rms difference = 0.47 Å for C_α atoms of the COMM domain, using the same superposition), showing that, apart from the COMM domain, the polypeptide backbone of the entire $\alpha\beta$ complex is in essentially the same conformation in $TRPS^{F-IPP}$ and $TRPS^{F-IPP}_{A-A}$ (Figure 9). Superposition of C_α atoms belonging to the COMM domain gives an rms difference of 0.23 Å with the positions of the COMM domains in $TRPS^{F-IPP}$ and $TRPS^{F-IPP}_{A-A}$ being related by a rotation of ≈2° approximately around the axis connecting βGly102-C_α and βGly189-C_α. This suggests the two residues act as hinges around which the entire domain pivots as a rigid body. Side chains within the COMM domain also show identical conformations, the only exceptions being βGln114, which moves together with PLP (Figure 8), and the aromatic ring of βPhe147, which loses contact with the second β-subunit in the $\alpha_2\beta_2$ complex. The rigid-body displacement of the COMM domain upon formation of the aminoacrylate is most likely caused by the interaction of the aminoacrylate carboxylate group with loop βL3 and leads to a slight stretching of most of the hydrogen bonds between helix βL6 and loop αL2 (Table 2). The resulting strain could be propagated to the scissile bond of the natural substrate of the α-site via the hydrogen bond between αAsp60-$O_{\delta 1}$ and the indole N_1 atom (Figure 6) and thereby activate the α-reaction.

Superposition of the β-subunits of the recently determined structure of the mutant βK87T complexed with IPP (*61*) and $TRPS^{F-IPP}_{A-A}$ reveals that, although most of the β-subunit retains an identical structure in the mutated protein, there are substantial differences in the conformation of the COMM domain in the $\beta135-\beta150$ and $\beta157-\beta166$ regions (Figure 10). Since Rhee et al. do not observe the aminoacrylate in the β-site, but rather the external aldimine (Figure 2), the additional interactions between the $O_{\gamma 1}$ of the external aldimine formed and loop βL3 may be a reason for these differences (Figure 11). However, they can also be a consequence of the replacement of βLys87 by threonine. In the βK87T mutant, the $O_{\gamma 1}$ atom of βThr87 expels a water molecule (Wat28), which, in the wild-type structure, provides two hydrogen bonds linking βThr88-$O_{\gamma 1}$ and βGlu114-$N_{\epsilon 2}$ that position βL3 relative to the backbone atoms of βLys87. These hydrogen bonds are replaced by a pair of hydrogen bonds originating from βThr87 (βThr87-$O_{\gamma 1}\cdots\beta$Glu114-O and βThr87-$O_{\gamma 1}\cdots\beta$Thr88-N) resulting in loop βL3 being pulled closer to the region $\beta87-\beta88$ by about 0.5 Å (Figure 11). The latter change, or possibly both changes together, lead to a chain reaction by which a completely new hydrogen bonding network is built up for the $\beta135-\beta144$ and $\beta156-\beta166$ regions, leading to a substantially different structure of the COMM domain. Clearly, this will have an effect on the allosteric interaction between the β- and the α-site and may thereby explain the much less pronounced activation of the α-reaction when, in the βK87T−IPP−Ser complex, the external aldimine is chemically converted to aminoacrylate (*39*).

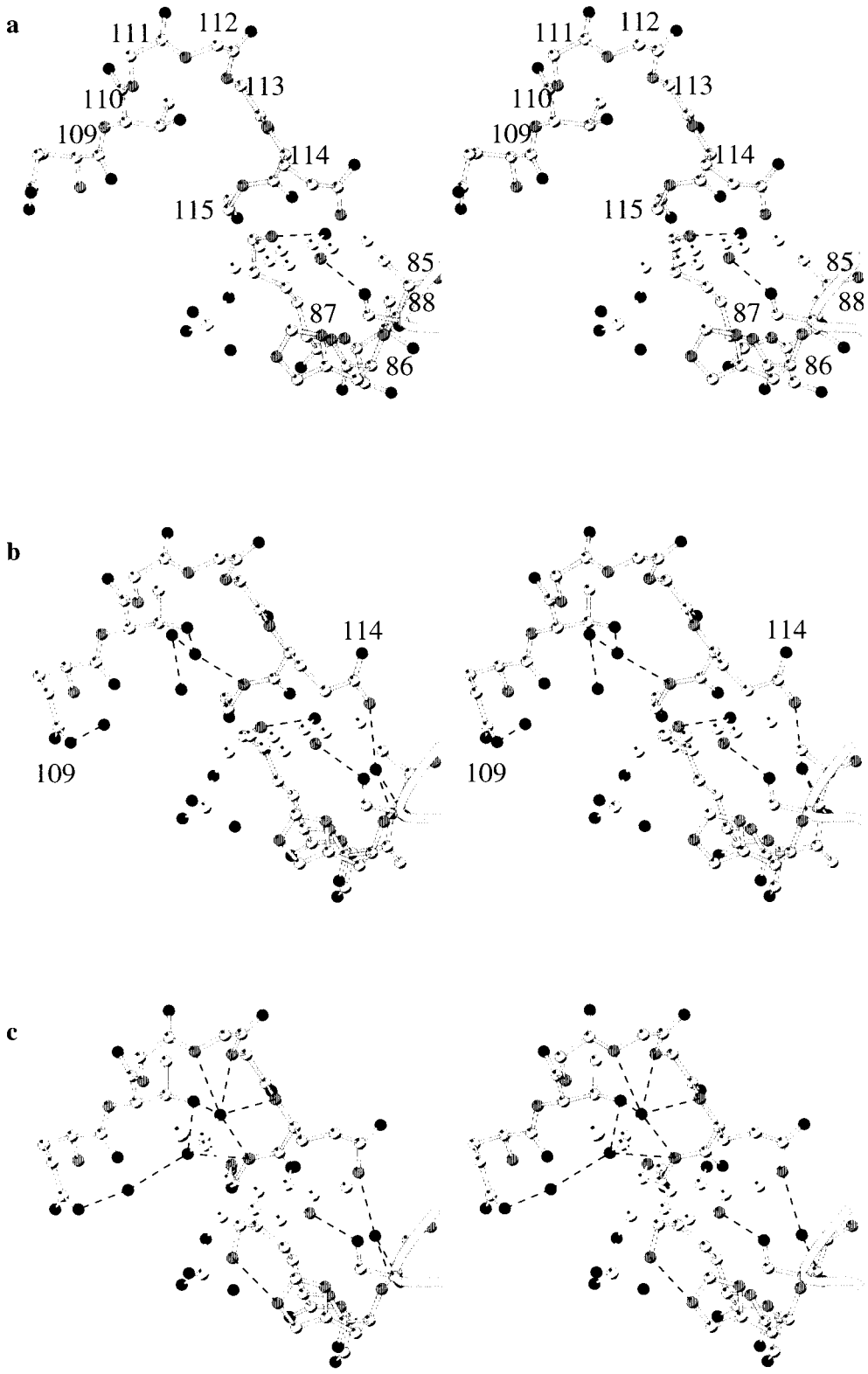

FIGURE 8: Ball-and-stick representation of the vicinity of the β-subunit cofactor PLP in (a) TRPS, (b) $TRPS^{F-IPP}$, and (c) $TRPS^{F-IPP}_{A-A}$. Carbon atoms and bonds belonging to the cofactor are shown in white and other carbon atoms and bonds in light gray. Nitrogen atoms are shown in dark gray and oxygen atoms in black. Hydrogen bonds are displayed as dashed lines. All interactions involving the phosphate group are omitted for clarity. In panel c, the C_β atom of the aminoacrylate is shown as a ball with a diameter larger than that of the other atoms. The figure was prepared using MOLSCRIPT (*34*).

Influence of the α*-Ligand on the Nature of the* β*-Ligand.* Spectroscopic studies have shown that binding of IPP, G3P, or phosphate to the α-active site shifts the distribution of enzyme-substrate intermediates at the β-active site to the aminoacrylate (*56*). In addition to the motion of loop βL3 relative to PLP discussed above, the position of the carboxylate group of βAsp305 with respect to the bound serine seems to play a major role. In the βK87T−Ser structure, the hydroxyl group of the external aldimine E(Aex_1) (see Figure 2) forms a hydrogen bond with the side chain

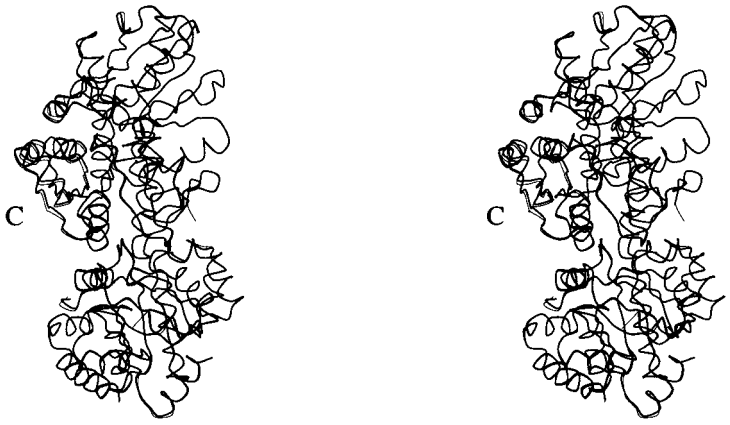

FIGURE 9: Superposition of $TRPS^{F-IPP}$ (thin line), and $TRPS^{F-IPP}_{A-A}$ (thick line) based on C_α atoms of residues not belonging to the COMM domain. The rms difference between the superpositioned C_α atoms is 0.24 Å. The orientation of the molecules is rotated 90° with respect to the orientation in Figure 1. The figure was prepared using MOLSCRIPT (*34*).

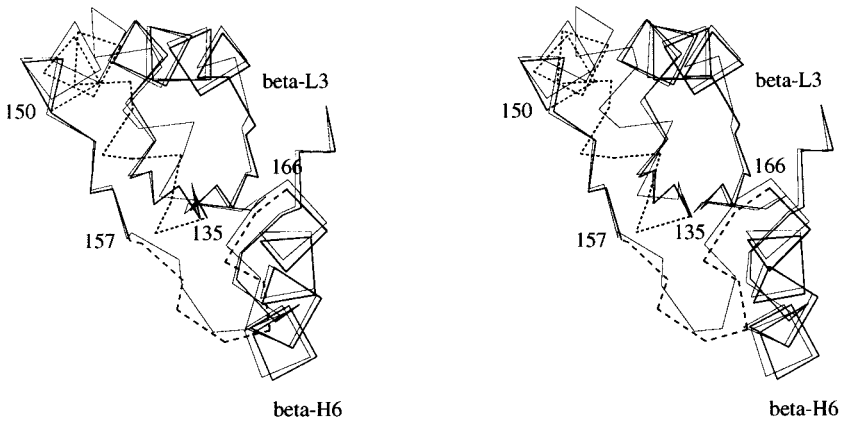

FIGURE 10: C_α traces of COMM domains from $TRPS^{F-IPP}_{A-A}$ (thick line) and the βK87T−IPP−L-Ser complex [thin line, PDB entry 2TRS (*61*)] after superposition of residues β10−β100 and β200−β380 using the program O (*30*). The regions exhibiting major conformational differences (β135−β150 and β157−β166) are shown as dashed lines. Helix β6 is marked. The figure was prepared using MOLSCRIPT (*34*).

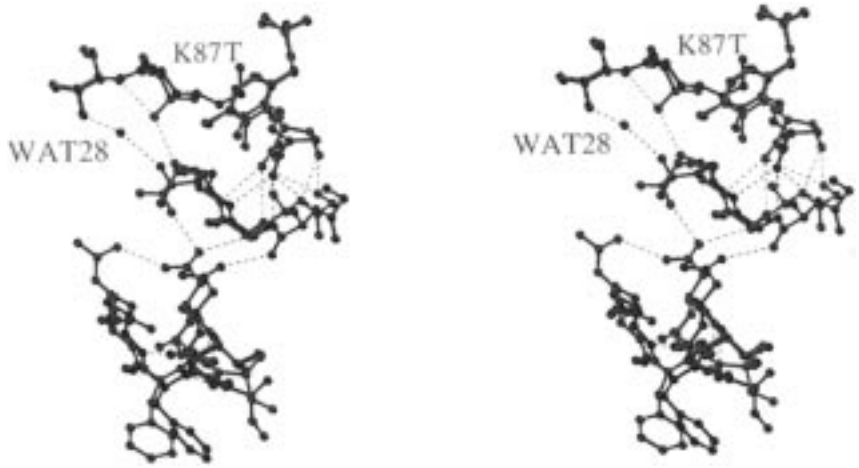

FIGURE 11: Ball-and-stick representations of the β-site from $TRPS^{F-IPP}_{A-A}$ (red) and the βK87T−IPP−L-Ser complex (PDB entry 2TRS, green) using the same superposition as in Figure 10. The C_α atom of residue β87 is marked. Hydrogen bonds are shown as dashed lines. The figure was prepared using MOLSCRIPT (*34*).

carboxylate of βAsp305 [2.7 Å distance, "swing-in" position (*61*)], stabilizing this intermediate. In both the wild-type and the βK87T mutant structures, the COMM domain moves upon binding of a ligand to the α-site and forces βAsp305 to move away from the swing-in position, most likely into the "swing-out" position where its carboxylate group points away from PLP (βK87T−Ser−GP, βK87T−Ser−IPP, and $TRPS^{F-IPP}_{A-A}$). There may be subtle differences in the driving forces for this transition due to the significantly different arrangement of some parts of the COMM domain between the wild type and the βK87T mutant. In the latter case, βAsp138 seems to destabilize the swing-in and βArg141 seems to stabilize the swing-out position after movement of the COMM domain. In wild-type TRPS, these two residues do not play a role. Here a close contact between $C_\alpha\beta$111 (part of loop βL3) and the swing-in position may trigger the

transition. The result is the same in both cases; after the loss of the interaction with βAsp305, water can protonate the E(Aex_1) hydroxyl group, and by elimination of a water molecule, the aminoacrylate is formed. This explanation is also consistent with the cation-specific distribution of the external aldimine and the aminoacrylate (*55*, *71*) since structures of TRPS complexed with either K^+, Cs^+, or Na^+ show that the βAsp305 position depends on the metal that is present (*60*). The importance of the βAsp305 side chain also becomes obvious when it is mutated to Asn (*3*).

Mechanism of the Tunnel. The tunnel connecting the α- and the β-site changes in several respects upon binding of F-IPP. The rearrangement of loop αL2 and helix βH6 leads to a complete blockage of the tunnel first by the ordered position of αL2 itself (Figure 5) and second by a concerted reorientation of the side chains of βTyr279 and βPhe280 into the position obstructing the tunnel, as previously found by Rhee et al. (*60*). This reorientation is facilitated by hydrogen bonds between the hydroxyl oxygen of βTyr279 and αAsp56-$O_{\delta 2}$, the amide group of βAsn171, and the carbonyl oxygen of βLys161 that are formed upon the concurrent ordering of loop αL2 and helix βH6.

How can the tunnel be made permeable after indole is produced by cleavage of the $C_3-C_{3'}$ bond of the α-subunit substrate? We speculate that αAsp60, one of the anchoring points of the closed conformation of loop αL2, gains conformational flexibility as soon as the bond between indole and G3P is broken. Strain built up prior to the bond cleavage is then released in a displacement of the COMM domain. Such a conformational change would result in loop αL2 opening the tunnel, while loop βL6 remains in its closed conformation preventing solvent access. Simultaneously, the hydrogen bonds between loop αL2 and the COMM domain responsible for keeping βTyr279 and βPhe280 in the "tunnel-blocked" position would be lost, allowing the two side chains to swing back into the "tunnel-open" position, thus rendering the tunnel fully permeable.

Conclusions. The results presented here allow the description of several important features of the catalytic cycle of tryptophan synthase in structural terms. Binding of an α-site substrate triggers the ordering of two previously disordered loop regions and thereby creates a reaction volume for the α-reaction that is secluded from both solvent and the tunnel leading to the β-site. Simultaneously, a newly defined domain, the COMM domain, becomes ordered and establishes a pathway by which information can be communicated allosterically from the α- to the β-site and vice versa. The actual communication between the two sites involves only a small number of key interactions bridging the intersubunit interface and connecting the COMM domain to the β-site, the transmitter between these being rigid-body displacements of the entire COMM domain. Two central steps of the catalytic cycle, the adjustment of the equilibrium at the β-site upon substrate binding at the α-site and the activation of the α-reaction after formation of aminoacrylate at the β-site, can be explained by this model. Related to these findings, a possible mechanism for control of the tunnel permeability is suggested.

ACKNOWLEDGMENT

We thank Ed Mitchell for providing a parameter set for PLP. We thank Klaus Scheffzek and Kelvin Chu for critical reading of the manuscript. We are grateful to Robert M. Sweet for continuous support.

REFERENCES

1. Ahmed, S. A., Miles, E. W., and Davies, D. R. (1985) *J. Biol. Chem. 260*, 3716−3718.
2. Ahmed, S. A., Hyde, C. C., Thomas, G., and Miles, E. W. (1987) *Biochemistry 26*, 5492−5498.
3. Ahmed, S. A., Ruvinov, S. B., Kayastha, A. M., and Miles, E. W. (1991) *J. Biol. Chem. 266*, 21548−21557.
4. Ahmed, S. A., McPhie, P., and Miles, E. W. (1996) *J. Biol. Chem. 271*, 29100−29106.
5. Anderson, K., Sikorski, J., and Johnson, K. (1988) *Biochemistry 27*, 1604−1610.
6. Anderson, K. S., Miles, E. W., and Johnson, K. A. (1991) *J. Biol. Chem. 266*, 8020−8033.
7. Banik, U., Zhu, D.-M., Chock, P. B., and Miles, E. W. (1995) *Biochemistry 34*, 12704−12711.
8. Berlyn, M. B., Last, R. L., and Fink, G. R. (1989) *Proc. Natl. Acad. Sci. U.S.A. 86*, 4604−4608.
9. Bernstein, F. C., Koetzle, T. F., Williams, G. J. B., Meyer, E. F., Jr., Brice, M. D., Rodgers, J. R., Kennard, O., Shimanouchi, T., and Tasumi, M. (1977) *J. Mol. Biol. 112*, 535−542.
10. Bork, P., and Rohde, K. (1990) *Biochem. Biophys. Res. Commun. 171*, 1319−1325.
11. Brünger, A. T. (1997) *X-PLOR 3.851*, Yale University Press, New Haven, CT.
12. Brzovic, P. S., Kayastha, A. M., Miles, E. W., and Dunn, M. F. (1992) *Biochemistry 31*, 1180−1190.
13. Brzovic, P. S., Ngo, K. N., and Dunn, M. F. (1992) *Biochemistry 31*, 3831−3839.
14. Brzovic, P. S., Sava, Y., Hyde, C. C., Miles, E. W., and Dunn, M. F. (1992) *J. Biol. Chem. 267*, 13028−13039.
15. Brzovic, P. S., Hyde, C. C., Miles, E. W., and Dunn, M. F. (1993) *Biochemistry 32*, 10404−10413.
16. Burley, S. K., and Petsko, G. A. (1988) *Adv. Protein Chem. 39*, 125−189.
17. Crawford, I. P. (1989) *Annu. Rev. Microbiol. 43*, 567−600.
18. Creighton, T. E. (1970) *Eur. J. Biochem. 129*, 561−570.
19. Crisanti, M., and Matthews, R. (1981) *Biochemistry 20*, 2700−2706.
20. Demoss, J. A. (1962) *Biochim. Biophys. Acta 62*, 279−293.
21. Heyn, M. P., and Weischet, W. O. (1975) *Biochemistry 14*, 2962−2968.
22. Hodel, A., Kim, S.-H., and Brünger, A. T. (1992) *Acta Crystallogr. A48*, 851−858.
23. Holm, L., and Sander, C. (1993) *J. Mol. Biol. 233*, 123−138.
24. Hur, O., Leja, C., and Dunn, M. F. (1996) *Biochemistry 35*, 7378−7386.
25. Hyde, C. C., Ahmed, S. A., Padlan, E. A., Miles, E. W., and Davies, D. R. (1988) *J. Biol. Chem. 263*, 17857−17871.
26. Hyde, C. C., and Miles, E. W. (1990) *Bio/Technology 8*, 27−32.
27. Jackson, A. H., and Naidoo, B. (1969) *Tetrahedron 25*, 4843.
28. Jackson, R. W., and Manske, R H. (1930) *J. Am. Chem. Soc. 52*, 5029−5034.
29. Jiang, J. S., and Brünger, A. T. (1994) *J. Mol. Biol. 243*, 100−115.
30. Jones, T. A., Zou, J. Y., Cowan, S. W., and Kjeldgaard, M. (1991) *Acta Crystallogr. A47*, 110−119.
31. Kabsch, W., and Sander, C. (1983) *Biopolymers 22*, 2577−2637.
32. Kirschner, K., Wiskocil, R. L., Foehn, M., and Rezeau, L. (1975) *Eur. J. Biochem. 60*, 513−523.
33. Kirschner, K., Lane, A. N., and Strasser, A. W. M. (1991) *Biochemistry 30*, 472−478.
34. Kraulis, P. (1991) *J. Appl. Crystallogr. 24*, 946−950.
35. Lane, A. N., and Kirschner, K. (1991) *Biochemistry 30*, 479−484.
36. Laskowski, R. A., MacArthur, M. W., Moss, D. S., and Thornton, M. T. (1993) *J. Appl. Crystallogr. 25*, 283−291.
37. Leja, C. A., Woehl, E. U., and Dunn, M. F. (1995) *Biochemistry 34*, 6552−6561.

38. Lolis, E., and Petsko, G. A. (1990) *Biochemistry 29*, 6619−6625.
39. Lu, Z., Nagata, S., McPhie, P., and Miles, E. W. (1993) *J. Biol. Chem. 268*, 8727−8734.
40. Matchett, W. H. (1974) *J. Biol. Chem. 249*, 4041−4049.
41. McDowell, L. M., Lee, M., Schaefer, J., and Anderson, K. S. (1995) *J. Am. Chem. Soc. 117*, 12352−12353.
42. McDowell, L. M., Lee, M., McKay, R. A., Anderson, K. S., and Schaefer, J. (1996) *Biochemistry 35*, 3328−3334.
43. Deleted in proof.
44. Miles, E. W., Phillips, R. S., Yeh, H. J. C., and Cohen, L. A. (1986) *Biochemistry 25*, 4240−4249.
45. Miles, E. W. (1991) *Adv. Enzymol. Relat. Areas Mol. Biol. 64*, 93−172.
46. Miles, E. W. (1995) *Subcell. Biochem. 24*, 207−254.
47. Mozzarelli, A., Peracchi, A., Rossi, G. L., Ahmed, S. A., and Miles, E. W. (1989) *J. Biol. Chem. 264*, 15774−15780.
48. Murzin, A. G., Brenner, S. E., Hubbard, T., and Chothia, C. (1995) *J. Mol. Biol. 247*, 536−540.
49. Nagata, S., Hyde, C. C., and Miles, E. W. (1989) *J. Biol. Chem. 264*, 6288−6296.
50. Nicholls, A., and Honig, B. (1993) *GRASP*, Columbia University, New York.
51. Noble, M. E. M., Wierenga, R. K., Lambeir, A. M., Opperdoes, F. R., Thunissen, A. M. W. H., Kalk, K. H., Groendijk, H., and Hol, W. G. J. (1991) *Proteins 10*, 50−69.
52. Otwinowski, Z., and Minor, W. (1997) *Methods Enzymol. 276*, 307−325.
53. Pan, P., and Dunn, M. F. (1996) *Biochemistry 35*, 5002−5013.
54. Pan, P., Woehl, E., and Dunn, M. F. (1997) *Trends Biochem. Sci. 22*, 22−27.
55. Peracchi, A., Mozarelli, A., and Rossi, G. L. (1995) *Biochemistry 34*, 9459−9465.
56. Peracchi, A., Bettati, S., Mozarelli, A., Rossi, G. L., Miles, E. W., and Dunn, M. F. (1996) *Biochemistry 35*, 1872−1880.
57. Petsko, G. A. (1985) *Methods Enzymol. 114*, 141−146.
58. Ramachandran, G. N., and Sasiekharan, V. (1968) *Adv. Protein Chem. 23*, 283−437.
59. Read, J. R. (1986) *Acta Cryst. A42*, 140−149.
60. Rhee, S., Parris, K. D., Ahmed, S. A., Miles, E. W., and Davies, D. R. (1996) *Biochemistry 35*, 4211−4221.
61. Rhee, S., Parris, K. D., Hyde, C. C., Ahmed, S. A., Miles, E. W., and Davies, D. R. (1997) *Biochemistry 36*, 7664−7680.
62. Rossi, G. L., Mozzarelli, A., Peracchi, A., and Rivetti, C. (1992) *Philos. Trans. R. Soc. London, Ser. A 340*, 191−207.
63. Ruvinov, S. B., Yang, X. J., Parris, K. D., Banik, U., Ahmed, S. A., Miles, E. W., and Sackett, D. L. (1995) *J. Biol. Chem. 270*, 6357−6369.
64. Sarker, K. D., and Hardman, J. K. (1995) *Proteins 21*, 130−139.
65. Silfhout, R. G., and Hermes, C. (1995) *Rev. Sci. Instrum. 66*, 1818−1820.
66. Strambini, G. B., Cioni, P., Peracchi, A., and Mozzarelli, A. (1992) *Biochemistry 31*, 7535−7542.
67. Stroud, R. M. (1994) *Nat. Struct. Biol. 1*, 131−134.
68. Tener, G. M. (1961) *J. Am. Chem. Soc. 83*, 159−168.
69. Wierenga, R. K., Noble, M. E. M., Postma, J. P. M., Groendijk, H., Kalk, K. H., Hol, W. G. J., and Opperdoes, F. R. (1991) *Proteins 10*, 33−49.
70. Wilmanns, M., Hyde, C. C., Davies, D. R., Kirschner, K., and Jansonius, J. N. (1991) *Biochemistry 30*, 9161−9169.
71. Woehl, E. U., and Dunn, M. F. (1995) *Biochemistry 34*, 9466−9476.
72. Wyckoff, H. W., Doscher, M., Tsernoglou, D., Inagam, T., Johnson, L. N., Hardman, K. D., Allewell, N. M., Kelly, D. M., and Richards, F. M. (1967) *J. Mol. Biol. 27*, 563−578.
73. Yang, X. J., and Miles, E. W. (1993) *J. Biol. Chem. 30*, 22269−22272.
74. Yanofsky, C., and Crawford, I. P. (1972) in *The Enzymes* (Boyer, P. D., Ed.) pp 1−31, Academic Press, New York and London.
75. Esnouf, R. M. (1997) *J. Mol. Graphics 15*, 132−134.

BI9728957